NASA Technical Memorandum 84315

Simulation of a Weather Radar Display for Over-Water Airborne Radar Approaches

George R. Clary

February 1983

NASA
National Aeronautics and
Space Administration

NASA Technical Memorandum 84315

Simulation of a Weather Radar Display for Over-Water Airborne Radar Approaches

George R. Clary, Ames Research Center, Moffett Field, California

NASA
National Aeronautics and
Space Administration

Ames Research Center
Moffett Field, California 94035

TABLE OF CONTENTS

Page intentionally left blank

SYMBOLS

BG	beacon gain setting, dB
c	speed of light (3.00×10^8 m/sec)
C_1, C_2, C_3	constants for sea clutter calculations
G	antenna gain, dimensionless
G_{dB}	antenna gain, dB
G_{beacon}	beacon antenna gain, dB
G_p	peak antenna gain, dB
L	one-way radar system loss, dimensionless
L_{dB}	radar system losses (one-way), dB
$P_R, P_{Rbeacon}, P_{Rsea}$	radar power received for primary targets, beacon targets, and sea clutter, respectively, W
P_T	radar power transmitted, W
$P_{Tbeacon}$	beacon power transmitted, W
R, R_{nm}	range to target; meters, n. mi.
R_B	range break point for display threshold calculations, n. mi.
RG	radar gain setting, dB
TILT	antenna tilt angle, deg
VWIND	wind speed, knots
θ_B	radar beam width, rad
λ	radar wavelength, m
λ_b	beacon reply wavelength, m
σ	target reflectivity, m^2
σ_s	average sea target reflectivity per unit area, dimensionless
τ	radar pulse duration, sec
ψ_{rel}	difference between antenna heading and sea heading, rad

SUMMARY

Airborne radar approach (ARA) concepts are being investigated as a part of NASA's Rotorcraft All-Weather Operations Research Program on advanced guidance and navigation methods. This research is being conducted using both piloted simulations and flight test evaluations. For the piloted simulations, a mathematical model of the airborne radar has been developed for over-water ARAs to offshore platforms. This simulated flight scenario requires radar simulation of point targets, such as oil rigs and ships, distributed sea clutter, and transponder beacon replies. Radar theory, weather radar characteristics, and empirical data derived from in-flight radar photographs are combined to model a civil weather/mapping radar typical of those used in offshore rotorcraft operations. The resulting radar simulation is realistic and provides the needed simulation capability for ongoing ARA research.

1. INTRODUCTION

The use of airborne weather/mapping radar as an approach aid is leading to increased development of airborne radar approach (ARA) concepts. ARAs have the advantages of minimal ground-based equipment, and the radar provides a means to ensure obstacle clearance for approach and missed approach segments. ARAs are in use for offshore helicopter operations to and from oil rigs, and the FAA has approved approach minimums of 200 ft radar altitude and 3/4 mile visibility on a limited basis. However, the flight crew workload is very high and flightpath tracking lacks precision.

As part of the Rotorcraft All-Weather Operations Research Program being conducted at the NASA-Ames Research Center, advanced concepts for enhancement of ARA are being studied with the goals of reducing crew workload, improving approach tracking precision, and reducing weather minimums. This program is being carried out through both simulation and flight test evaluations.

An initial step in the simulation phase of this program has been to develop the hardware and software necessary to simulate the airborne weather/mapping radar. This simulation allows ARA concepts to be developed and examined using a fixed-base helicopter simulator prior to flight test evaluation. Additional capability is being developed to display a variety of symbols and alphanumeric characters on the radar and also to simulate overland approach displays.

The over-water radar scenario is characterized by a scattering of point targets, such as oil rigs and ships, which are surrounded by large ocean areas with much lower radar reflectance. Mathematical models for point target returns and distributed sea clutter returns have been developed as described herein. These models are derived from radar theory and are combined with the design characteristics of the Sperry/RCA Primus 500 color weather radar. Comparisons of the simulated display with in-flight radar display photographs provide a means of validating the authenticity of the displayed video. These in-flight data were also useful in determining reasonable ways to simulate sea clutter within the time constraints for real-time computational algorithms.

A demonstration of how the combination of radar theory, weather radar characteristics, and data extracted from in-flight radar display photographs were used for simulating the radar video display is included in this paper. Photographs which show the degree of realism obtained with the radar simulation are also included. Detailed

documentation on the actual computer software used for generating the simulated radar display is contained in reference 1.

2. REVIEW OF RADAR THEORY

The radar simulation mathematically models target return intensities using standard radar equations (ref. 2). For this simulation, three types of targets are simulated: (1) point targets representative of offshore oil rigs are considered; (2) X-band transponder beacon targets, such as the portable beacons currently in use to aid in oil rig identification, are simulated; and (3) broad areas of sea clutter are simulated. The radar equations applicable to each of these types of targets are described in sections 2.1, 2.2, and 2.3, respectively.

2.1 Point Targets

Oil rig and ship target returns are modelled as point reflectors with constant reflectivity. The basic equation for the power received at the radar receiver/transmitter is from section 1.2 of reference 2 and is

$$P_R = \frac{P_T G^2 \lambda^2 \sigma}{(4\pi)^3 R^4 L^2} \tag{1}$$

where

P_R power received, W

P_T power transmitted, W

G antenna gain

λ radar wavelength, m

L one-way radar system losses

σ target reflectivity, m^2

R range to target, m

Equation (1) is more conveniently expressed in logarithmic form, so that many of the parameters are in decibels (dB). In this form, power units of decibels above a milliwatt (dBm) are used. Therefore, equation (1) becomes

$$P_R(\text{dBm}) = P_T(\text{dBm}) + 2G_{dB} - 2L_{dB} + 20 \log \lambda + 10 \log \sigma - 30 \log 4\pi - 40 \log R \tag{2}$$

Typical values for the inputs are

P_T 7000 W = 68.45 dBm

λ 0.0320 m (for a 9375 MHz, X-band radar)

σ 1000 m^2 for a typical oil rig (ref. 3, section 2.2.2.11)

With these values for P_T, λ, and σ and with range expressed in nautical miles, equation 2 reduced to

$$P_R(\text{dBm}) = -95.13 - 40 \log R_{nm} + 2G_{db} - 2L_{dB} \quad (3)$$

Equation (3) forms the basis for the radar simulation of oil rig targets. The antenna gain is calculated based on antenna patterns and the angular error between the target location and the antenna pointing direction (sec. 3.2). Losses are based on the factors discussed in section 3.2. Then, given the range to a target and the antenna pointing geometry relative to the target (including both azimuth and elevation pointing errors), the received power can be calculated. Once this power has been determined, the video display intensities are determined based on system-specific sensitivity time control (STC) characteristics and color video trigger levels as described in section 3.3.

2.2 Transponder Returns

A second type of target return which can be simulated is one from a ground-based radar transponder. These transponder beacons are used to provide an effective means of identifying particular oil rigs. For purposes of this simulation, the characteristics of a Vega Model 367X transponder beacon are simulated.

The transponder operates on the principle of replying to certain X-band radar interrogations. To respond, the interrogating signal at the transponder must be greater than -65 dBm with a pulse width between 1.6 and 3.8 μsec. To simplify the radar simulation, the beacon is assumed to respond whenever it is interrogated with a 2.35 μsec pulse. Therefore, no calculations for the interrogation signal level received at the beacon are performed. This simplification results in no loss of fidelity for ranges to 100 n. mi.

The transponder beacon replies with a 9310 MHz, 400 W (56.02 dBm) transmitted signal 6.0 μsec after interrogation. The transponder return power received at the aircraft will be

$$P_{Rbeacon} = P_{Tbeacon} + G_{beacon} + G_{dB} + 20 \log \lambda_b - 20 \log 4\pi - 20 \log R - L_{dB} \quad (5)$$

where

$P_{Tbeacon}$ beacon power transmitted = 400 W = 56.02 dBm

G_{beacon} beacon antenna gain = 5 dB

λ_b beacon reply wavelength = 0.0322 m

Upon substitution of values for $P_{Tbeacon}$, G_{beacon}, and λ_b, equation (5) reduces to

$$P_{Rbeacon} = -56.16 - 20 \log R_{nm} + G_{dB} - L_{dB} \quad (6)$$

Equation (6) forms the basis for beacon target simulation. For this simulation, additional identification beacon pulses are not simulated. The video for beacon targets is displayed 0.5 n. mi. further in range than a corresponding primary target would be

because of the 6.0 μsec delay inherent in the transponder reply characteristics. Photographs of actual and simulated beacon targets are presented in section 5.2.

2.3 Sea Clutter

Sea clutter can limit the ability of airborne radar to detect targets, and it increases the radar operator workload for gain adjustments. However, simulation of sea clutter characteristics can be complex, mainly because of ever changing local sea surfaces. For this radar simulation, a simplified sea clutter representation has been derived and implemented. This clutter model enhances the operational fidelity of the radar simulation and represents a compromise between functional realism and display-generation speed.

The magnitude of the sea clutter echo returned to the radar receiver depends on the radar characteristics, the grazing angle of the radar beam, and the sea surface. The sea surface may be considered as composed of a number of individual small targets that vary in radar reflectivity and that reflect the incident radar energy. With the discussion in section 12.3 of reference 2 as a guide, a dimensionless average sea target reflectivity per unit area, σ_s, is defined. This average sea reflectivity is multiplied by the sea area illuminated by a radar pulse to obtain sea reflectance in units of square meters. (Note that σ_s, being dimensionless, is expressed in dB.) Next, by restricting the discussion to the small grazing angles used for ARA work, the average returned power from an ocean area at range, R, is expressed as

$$P_{Rsea} = \frac{P_T G^2 \lambda^2 \theta_B c \tau \sigma_s}{(4\pi)^3 2 R^3 L^2} \tag{7}$$

where

P_T, G, λ, L are the power transmitted, antenna gain, radar wavelength, and one-way losses, respectively

θ_B radar beamwidth, rad

c speed of light = 3.00×10^8 m/sec

τ radar pulse duration, sec

The sea reflectivity, σ_s, depends on grazing angle, wave height, and sea direction. Increasing grazing angle from 1° to 10° increases σ_s by 3 to 10 dB, depending on sea conditions. Wave height effects are difficult to quantify. In general, measurements show that σ_s increases as the sea becomes rougher, but at larger wave heights σ_s does not increase as rapidly as it does at smaller wave heights. Combining this characteristic with wind speed versus wave height characteristics suggested that σ_s be modelled as a linear function of wind speed. In addition, the sea reflectivity is 5 to 10 dB greater when looking into the waves (head sea) than it is in the opposite direction (down sea).

By using the above data, a sea clutter model was developed for the simulation. Sea clutter is not displayed when the antenna tilt is set above 2° or when the beacon mode of the radar is selected. Actual sea clutter photographs were used to help select some of the factors relating σ_s to the sea conditions. The resulting equation for sea reflectivity is

$$\sigma_s = -40 - C_1*TILT - C_2*|\psi_{rel}|/\pi + C_3*VWIND \quad (8)$$

where

C_1 tilt multiplier = 1.0 dB/deg

C_2 relative sea heading multiplier = 7 dB

C_3 wind multiplier = 0.15 dB/knot

TILT antenna tilt angle, deg ($-15 \leq TILT \leq 2$)

ψ_{rel} difference between the antenna heading and sea heading ($\psi_{rel} = 0$ for head sea, π for down sea)

VWIND wind speed, knots

Equations 7 and 8 are then used to calculate the average sea power returned. Sea direction is set equal to wind direction for wind speeds in excess of 5 knots. When wind speed is less than 5 knots, the sea is assumed to be random, making σ_s independent of heading. Once the average sea power returned, P_{Rsea}, has been calculated, it is compared with the level 1 radar video threshold (sec. 3.3), and if it is greater, a band of clutter is displayed. The clutter band is centered about the range where the radar beam centerline intersects the ocean surface, with the length of the band determined by the magnitude of the sea power returned. Randomness is introduced into the sea clutter appearance using a random noise function.

Figure 1 shows the simulated display with a band of clutter surrounding an oil rig target. Additional simulated clutter photos are shown in section 5 along with comparable in-flight radar displays.

3. CHARACTERISTICS OF THE AIRBORNE RADAR

This section discusses the weather/mapping radar characteristics which are specific to the NASA radar. This radar was built by Sperry/RCA Avionics, under contract to NASA. The radar system has been flown in two NASA aircraft, a Learjet 24 and a Sikorsky SH-3 helicopter, and the losses and antenna characteristics for these installations are discussed.

3.1 General System Description

The weather/mapping radar which is being modelled uses standard weather radar technology, but uses operational features which are useful for helicopter radar approaches. An RCA Primus 400 radar system was modified with operational features of the RCA Primus 50 radar along with other modifications. Display selectable range scales of 2.5, 5, 10, 25, 50, 100, and 200 n. mi. were incorporated. This experimental radar system is similar to the new Sperry Primus 500 weather/mapping radar.

Figure 2 shows the indicator and radar controls. The operating mode push buttons include ground mapping, weather, and weather cyclic modes. The ground mapping and weather modes differ in pulse width and display video trigger levels. A

three-position rotary switch allows display selection of primary radar returns only, beacon returns only, or both beacon targets and primary radar returns. Rotary knobs are provided for adjustment of radar gain, beacon gain, antenna tilt, and range scale. Four additional push buttons, two on each side of the cathode ray tube (CRT), are used to (1) select ±30 or ±60 sweep, (2) display an azimuth grid on the CRT, (3) freeze the display video, and (4) send a camera control signal.

3.2 Antenna Characteristics and Installation Losses

The Sperry/RCA radar system is available with both 12 and 18 in. diam antennas, and the simulation is set up to model any size circular antenna. For NASA flight testing, a 12 in. antenna is used in the Learjet and an 18 in. antenna is used in the SH-3 helicopter. The losses differ for the two aircraft as is discussed later in this section.

The antennas are circular, flat plate antennas with horizontal polarization. The data supplied by RCA (fig. 3) show the horizontal radiation pattern with scales for both the 12 and 18 in. antennas. The peak gain is quoted as +28 dB for the 12 in. antenna and +31.5 dB for the 18 in. antenna. These gains represent the gain above that of an isentropic radiator. Although vertical patterns were not available, for simulation purposes they are assumed to be identical in form to the horizontal patterns.

Another factor of significance for modeling the antenna patterns is the beam shape distortion effect of the radomes. Although quantitative distortion data are not available, study of oil rig radar returns using the Learjet imply a beamwidth that is about 15% wider than would be expected using the 12 in. diam antenna. This beam widening is currently attributed to radome distortion, and is incorporated into the radar simulation by specifying a constant beam-widening factor. The Learjet radome beamwidth distortion factor is estimated at 15%, and the SH-3 factor is estimated at less than 5%. These radome distortion factors are applied to the antenna patterns shown in figure 3 in simulating the transmitted and received radiation patterns.

The radar simulation also requires input of the losses associated with transmitting and receiving the radar signals. Losses include transmission line losses, rotary joint losses, radome losses, and weather penetration losses. Estimated losses for the NASA Learjet and SH-3 radar installations are shown in table 1. The radome losses were measured in tests performed by the Norton Company in Ohio, and the figures shown in table 1 represent these measured average radome losses. The transmission line and rotary joint losses are based on data from Sperry/RCA.

3.3 Display Intensities

The power returned from a given target can be determined by using the equations given in section 2, given the antenna pointing geometry and the antenna, radome, and loss parameters. Once this radar power returned has been calculated, the display intensity of the target must be determined. For the NASA color radar, three display intensities are used, with each intensity displayed in a different color as shown in table 2. An exception to this is that simulated sea clutter is always displayed at level 1 intensity (green or blue). The radar receiver uses a sensitivity time control (STC) to vary the display threshold levels as a function of target range. Also, radar gain, receiver/transmitter adjustments for antenna size, and radar operating modes

affect the display threshold levels. Graphs of the video threshold levels were obtained from Sperry/RCA Avionics for the Primus 500 radar. This information, combined with some assumptions to fill in the threshold data for operating modes where data were not supplied, has been modelled.

The video threshold levels for the display intensities are calculated based on the range, radar gain, and antenna size, given the operating mode (WX or MAP). Data for the threshold levels in the weather mode are shown in figure 4 for both 12 and 18 in. antennas. When changing from one antenna to the other, the receiver/transmitter is adjusted to obtain the characteristics shown. In principle, the threshold levels in the weather mode are chosen so that when in preset radar gain, a 3 mile diameter storm with rainfall rates of 1, 4, and 11.5 mm/hr would be displayed at Level 1, 2, and 3, respectively, independent of range.

For the radar simulation, the threshold levels of figure 4 have been fitted with equations. The weather display thresholds are divided into three regions, close-in, medium and long ranges. For close-in ranges, the thresholds decrease about 7 dB per octave increase in range. At medium range, they decrease at 12 dB per octave, and at long ranges, the trigger levels are constant at minimum discernable signal (MDS) levels. Radar gain adjustments have the effect of moving the close-in and medium range thresholds up and down, but MDS is independent of radar gain setting. Radar gain is adjustable using a knob on the front of the radar indicator, and the adjustment range is from a maximum of +3 dB above preset gain to 40 dB below preset.

In equation form, the weather operating mode display threshold levels of figure 4 are expressed as shown in equations (9)-(12). The break point, R_B, dividing close-in and medium range modes is calculated based on the antenna peak gain. When the antenna peak gain is determined, the Level 3 threshold is then calculated. The Level 2 and Level 1 thresholds are 7 dB and 17 dB, respectively, less than the Level 3 threshold.

$$R_B = 10^{(-2.4+G_p)/16.86} \tag{9}$$

$$\text{Level 3} = \begin{cases} -85.4 + G_p - 23 \log R_{nm} - R_G & R_{nm} \leq R_B \\ -87.8 + 2G_p - 39.86 \log R_{nm} - R_G & R_{nm} > R_B \end{cases} \tag{10}$$

Level 3 is constrained to be $\geq$-104 dB

$$\text{Level 2} = \text{Level 3} - 7.0 \text{ dB} \tag{11}$$

Level 2 is constrained to be $\geq$-106 dB

$$\text{Level 1} = \text{Level 3} - 17.0 \text{ dB} \tag{12}$$

Level 1 is constrained to be $\geq$-109 dB

where

R_B range break point, n. mi.

G_p peak antenna gain, dB

R_{nm} target range, n. mi.

RG radar gain setting, dB

The trigger levels in the map operating mode for preset gain are shown in figure 5. These trigger levels are set so that the target intensity in weather and map is the same at the 1/10 beam-filling range (for a 3 mile diameter storm cell), and the map mode trigger levels decrease 9 dB per octave increase in range until they reach the MDS levels. A general form for these trigger levels is shown in equations (13)-(15). Note that the MDS is a function of the radar pulse width so that in map mode on range scale settings below 50 n. mi., the MDS levels are higher than they are on the longer range scales. Also, the longer pulse width applies on all ranges when the radar is operated in both radar-plus-beacon or beacon-only modes.

$$\text{Level 3} = -92.33 + 1.333\, G_p - 29.90 \log R_{nm} - R_G \tag{13}$$

$$\text{Level 3 is constrained to be} \geq \begin{cases} -104 \text{ dB with } \tau = 2.35 \text{ μsec.} \\ -91 \text{ dB with } \tau = 0.6 \text{ μsec.} \end{cases}$$

$$\text{Level 2} = \text{Level 3} - 7.0 \text{ dB} \tag{14}$$

$$\text{Level 2 is constrained to be} \geq \begin{cases} -106 \text{ dB with } \tau = 2.35 \text{ μsec.} \\ -93 \text{ dB with } \tau = 0.6 \text{ μsec.} \end{cases}$$

$$\text{Level 1} = \text{Level 3} - 17.0 \text{ dB} \tag{15}$$

$$\text{Level 1 is constrained to be} \geq \begin{cases} -109 \text{ dB with } \tau = 2.35 \text{ μsec.} \\ -96 \text{ dB with } \tau = 0.6 \text{ μsec.} \end{cases}$$

where

G_p peak antenna gain, dB

R_{nm} target range, n. mi.

RG radar gain setting, dB

τ radar pulse duration

There is also a display threshold level for beacon targets. The beacon threshold is

$$\text{Beacon threshold} = -51.0 - 20.0 \log R_{nm} - BG \tag{16}$$

where

R_{nm} range to target (beacon), n. mi.

BG beacon gain setting, dB

The beacon gain is pilot adjustable over a range from +3 to -37 dB. For purposes of the simulation, no MDS beacon threshold is calculated since the 400 W transponder being simulated is detectable at all ranges of interest. However, if lower power transponders are simulated, a beacon MDS constraint of -83 dBm should be used.

4. COMPARISON OF AIRBORNE AND SIMULATED DISPLAYS

Video display radar returns of oil rigs and sea clutter were obtained in flight using a NASA Learjet. This data proved to be useful in developing and validating the simulated radar model. Although many simplifications have been made in modelling the radar, the resultant mathematical model presents a good representation of the airborne radar.

4.1 Airborne Radar Flight Description

This section describes the test flight on which radar simulation validation data was obtained. The flight objective was to obtain test data on the appearance of oil rig and beacon targets on the color radar. Target size, shape, and coloring as functions of range, radar gain, and radar operating mode (weather vs map) were recorded photographically.

The flight was performed using the NASA Learjet 24, NASA 705, with the radar equipment installed as described below. Radar images of oil rigs and sea clutter were photographed during a series of four low approaches to a group of 10 offshore oil rigs southeast of Santa Barbara, Calif. Beacon image data were recorded upon return to Moffett Field by interrogating a transponder beacon located a few hundred yards north of the NASA ramp.

The radar installation on the Learjet included a 12 in., flat plate antenna, the modified Sperry/RCA receiver/transmitter and color display, and a radar repeater scope. The active radar display was cabin-mounted in the experimenter's rack, and the repeater display was installed in the instrument panel for pilot reference.

The low approach profiles to the oil rigs are shown in figure 6, and they followed procedures similar to those used for helicopter ARAs. The approaches started 20 to 30 n. mi. from the destination rig. By using the altitude profile shown in figure 6, an approach angle of $1/2° \pm 1/2°$ was maintained, requiring almost no radar tilt adjustments throughout the approaches. The major difference between the approach profiles flown in this test and typical helicopter ARA profiles was airspeed, with the Learjet approaches flown at 150 knots indicated airspeed, compared with typical helicopter ARA speeds of 60 knots.

The weather conditions for this test were VFR, with no cloud cover and ground visibilities estimated at 20 miles. The Santa Barbara surface winds were initially reported as 180° at 7 knots, later changing to 240° at 12 knots.

Following a refueling stop, the aircraft returned to Moffett Field, gathering beacon return data beginning 75 n. mi. southeast of Moffett Field. For these tests, a Vega Model 367X X-band radar transponder with 400 W transmitting power was used. The beacon was set on Code 0, a code which pulses twice, the first pulse producing the beacon image and the second pulse producing an identifying image appearing 20 n. mi. further away.

4.2 Comparison Photographs

The airborne radar display photographs taken during the flight provided an excellent data source for validating the simulated display fidelity. The goals of the simulation were to provide pilots with a realistic experience with ARA tasks such as target identification, gain and tilt adjustment, and beacon delay interpretation. As shown in the comparison figures, these radar simulation fidelity goals were achieved.

Figure 7 contains a series of 12 pairs of photographs which demonstrate the capability of the radar simulation. The photographs show comparisons of simulated radar imagery with the imagery obtained in-flight with oil rig targets, sea clutter, and the ground transponder. Photographs 7(a) through 7(d) demonstrate the fidelity of oil rig target appearances in both the MAP and WX modes, with the radar gain in the "preset" position. Photographs 7(e) through 7(h) demonstrate the effects of gain adjustment, showing first low gain then high gain settings. For the low gain settings, the gain was adjusted to the lowest setting at which the oil rigs were consistently visible. The effects of sea clutter are evident in photographs 7(i), 7(j), and 7(k) for the fourth Learjet approach which was into the wind more than the previous approaches. The simulated sea clutter is slightly more sensitive to the WX or MAP mode setting than the actual radar as is evident by comparing figures 7(i) and 7(j). Figure 7(l) shows a typical beacon target display.

Comparison of these photographs shows that the effects of all of the radar controls are closely matched between simulated and in-flight displays. The color trigger levels, radar gain, and antenna pointing error effects are particularly realistic. Oil rig target shaping is good at ranges less than 2.5 miles, but at longer ranges the simulated targets are more box-shaped and have edges that are better defined. The sea clutter appearance is surprisingly good, considering the simplicity of the model. The simulated sea clutter characteristics of a single band of Level 1 clutter with irregular edges seems to provide a realistic video picture. Beacon target representation is excellent, but the beacon gain in the aircraft has been found more difficult to adjust because of gain control noise and suspected nonlinearities.

5. CONCLUSIONS

A simulation capability for over-water airborne radar approaches has been developed. This capability will be used for research and development programs to enhance ARA. A high degree of realism was obtained with the simulated radar display for over-water flight scenarios. The simulation is configured to display point targets such as oil rigs or ships, beacon targets, and sea clutter. Mathematical models for the radar power returned for these types of targets were developed. These models, combined with hardware-specific characteristics of the weather/mapping radar being used at NASA-Ames for advanced concept ARA programs, form the basis for digital simulation of weather/mapping radar video. The fidelity of the resulting simulated display has been validated by comparing in-flight photographs with photographs of the simulated radar display. This simulation will be a valuable resource for future ARA research.

6. REFERENCES

1. Karmarkar, J.; and Clark, D.: Real Time Simulation of an Airborne Radar for Overwater Approaches. NASA CR-166293, March 1982.

2. Skolnik, M. I.: Introduction to Radar Systems. McGraw-Hill Book Co., Inc., 1962.

3. Minimum Operational Performance Standards for Airborne Radar Approach and Beacon Systems for Helicopters. Radio Technical Commission for Aeronautics, Washington, D.C., Document No. RTCA/DO-172, November 1980. Prepared by SC-133.

TABLE 1. RADAR SYSTEM LOSSES

Source of loss	Estimated loss (one-way), dB	
	SH-3	Learjet
Radome	0.5	1.55
Transmission line	.8	.8
Rotary joints	.5	.5
Weather	Negligible (less than 0.1 dB/n. mi.)	
Total one-way loss	1.8	2.85

TABLE 2. COLOR RADAR DISPLAY INTENSITIES

Display intensity	Operating mode	Display color
0	All	Black (not visible)
1	WX	Green
	MAP	Blue
2	WX	Yellow
	MAP	Yellow
3	WX - radar only	Red
	MAP - radar only	Magenta
	WX - radar and beacon[a]	Yellow
	MAP - radar and beacon	Yellow

[a]Beacon targets are always displayed using white.

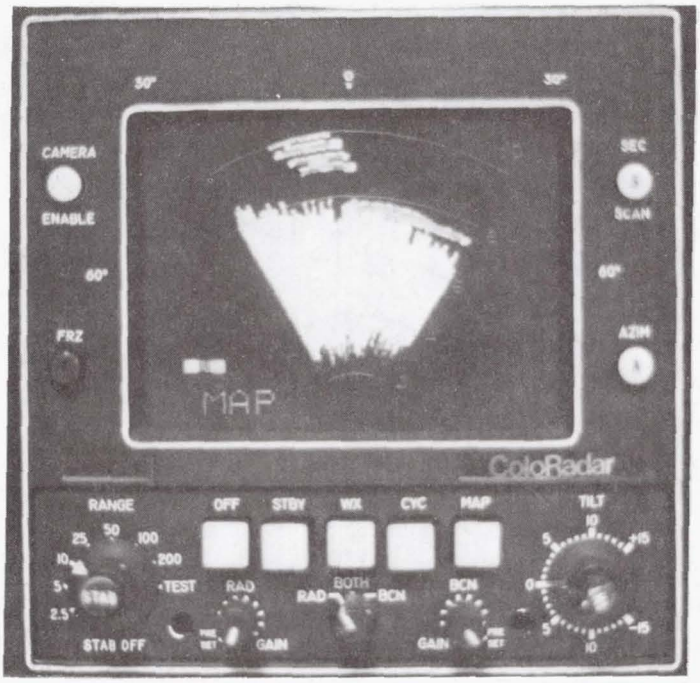

Figure 1.- Typical simulated radar display with oil rig targets and sea clutter.

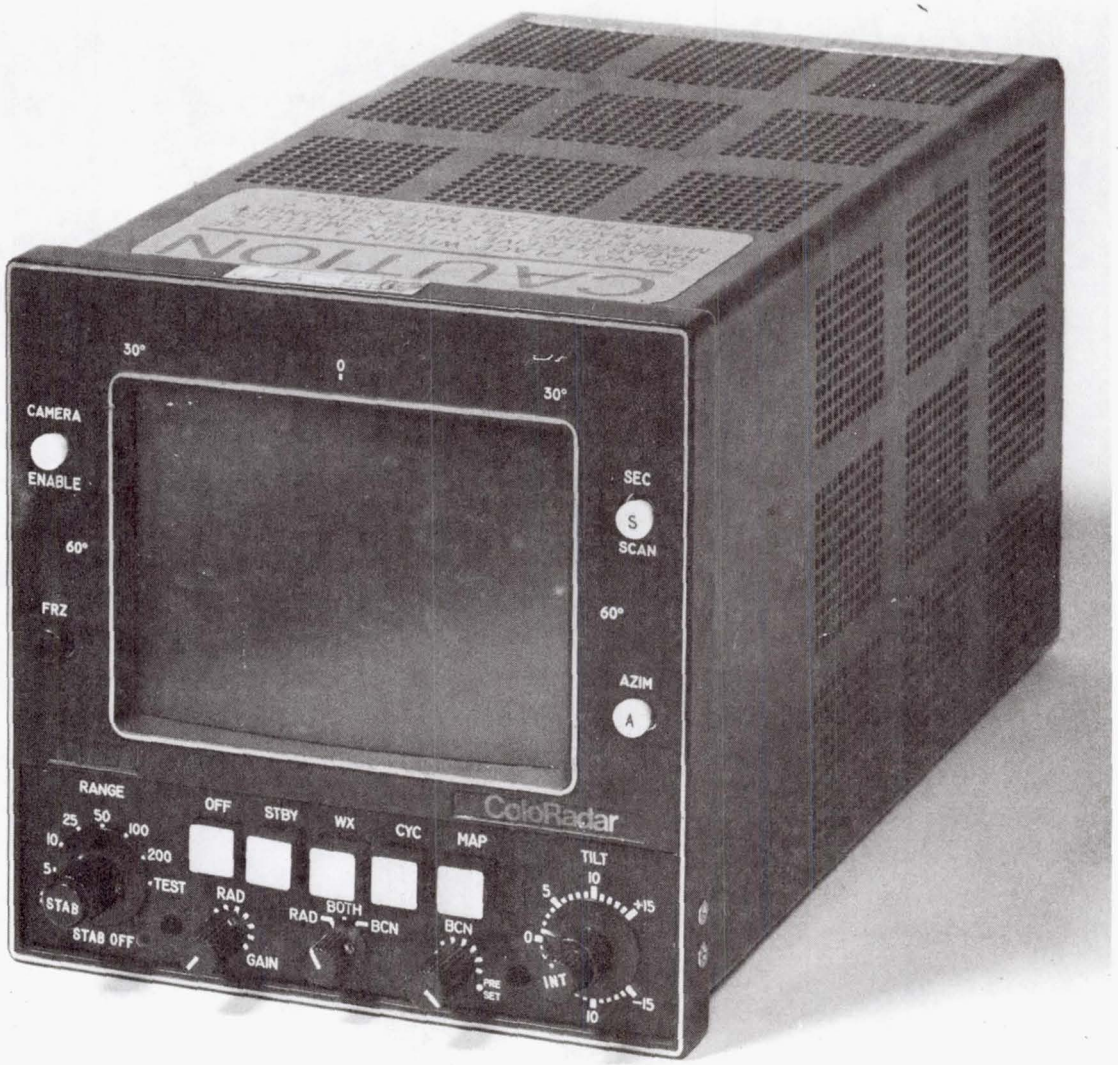

Figure 2.- Radar indicator.

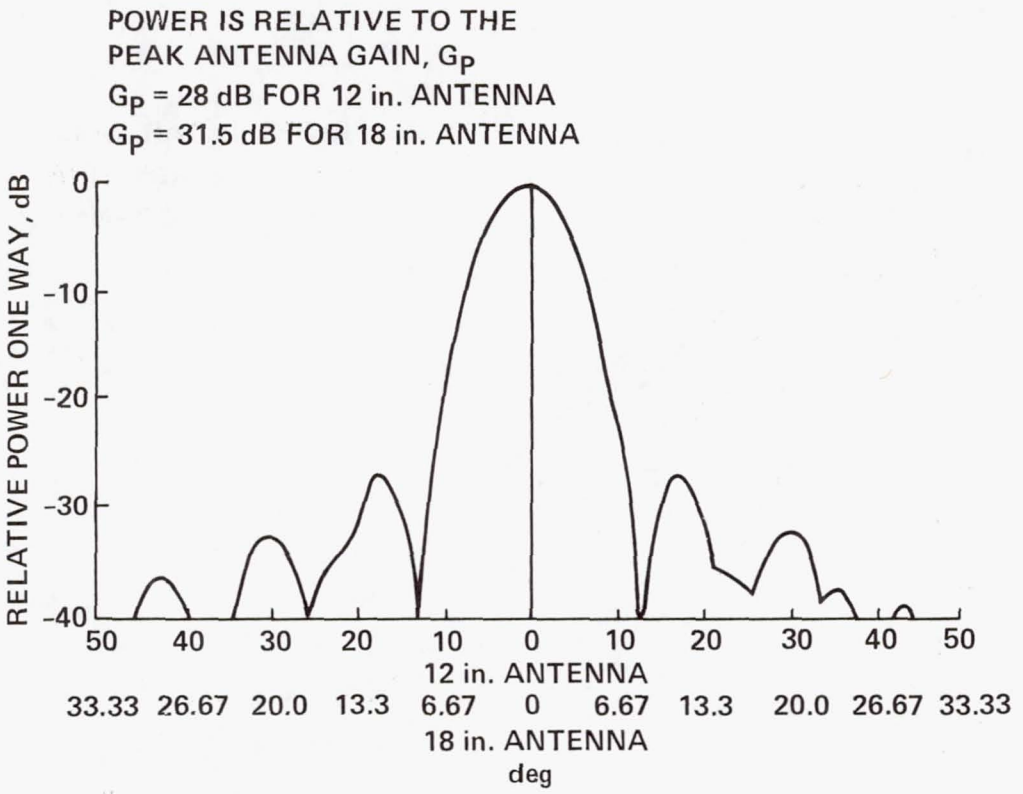

Figure 3.- Antenna pattern for the circular, flat plate antennas.

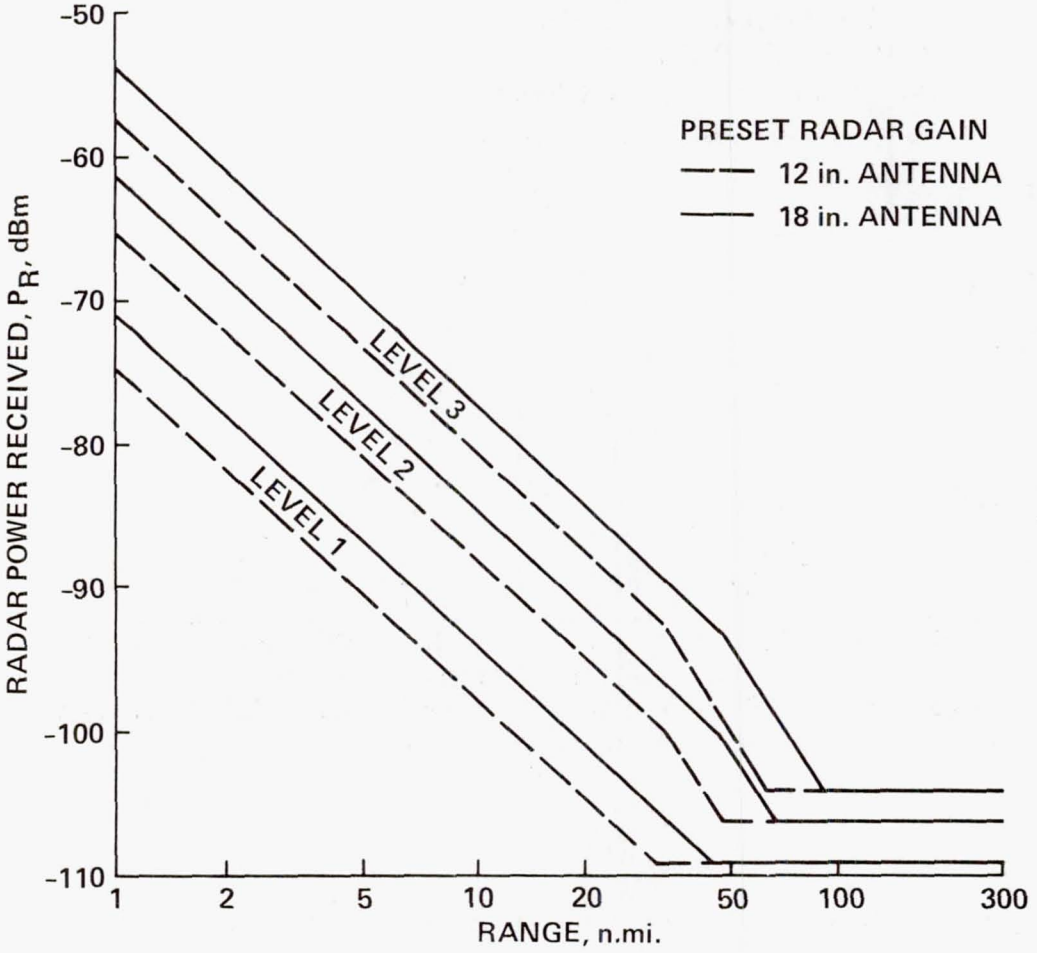

Figure 4.- Video threshold levels in the weather mode.

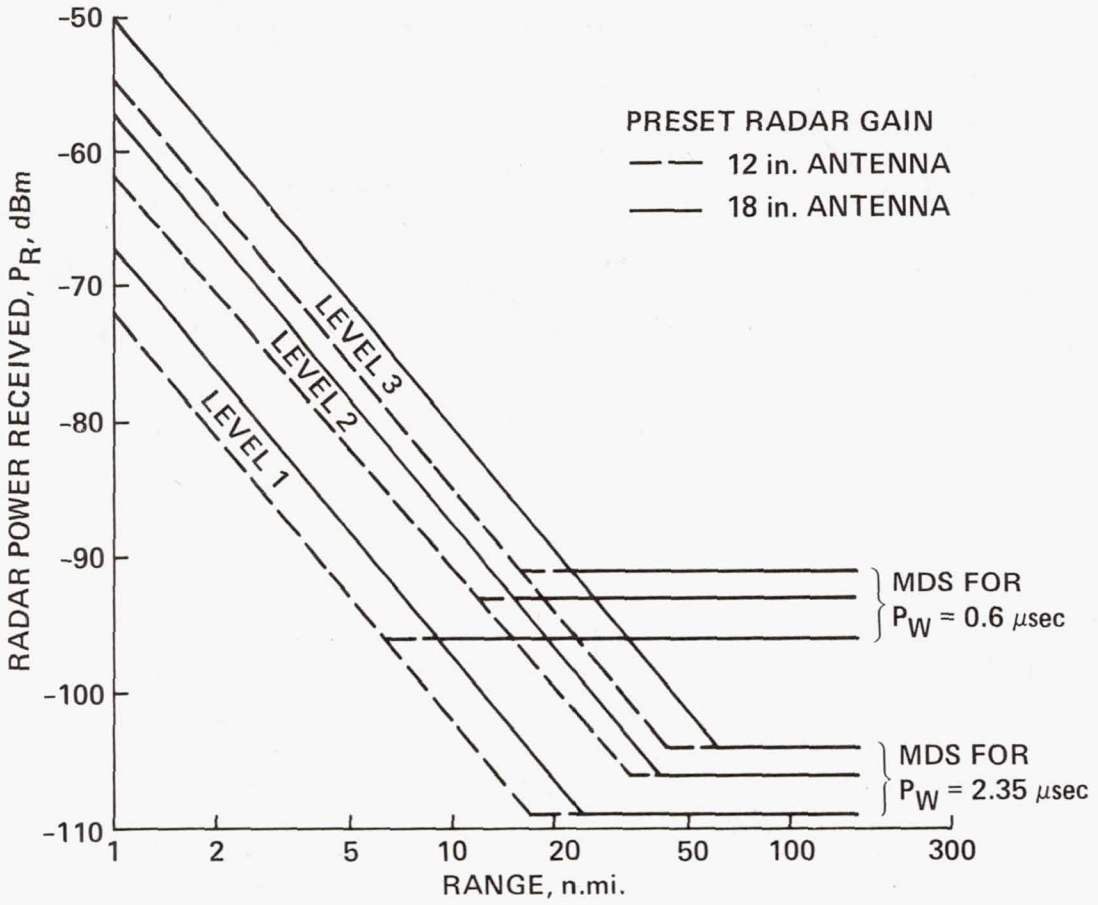

Figure 5.- Video threshold levels in the MAP mode.

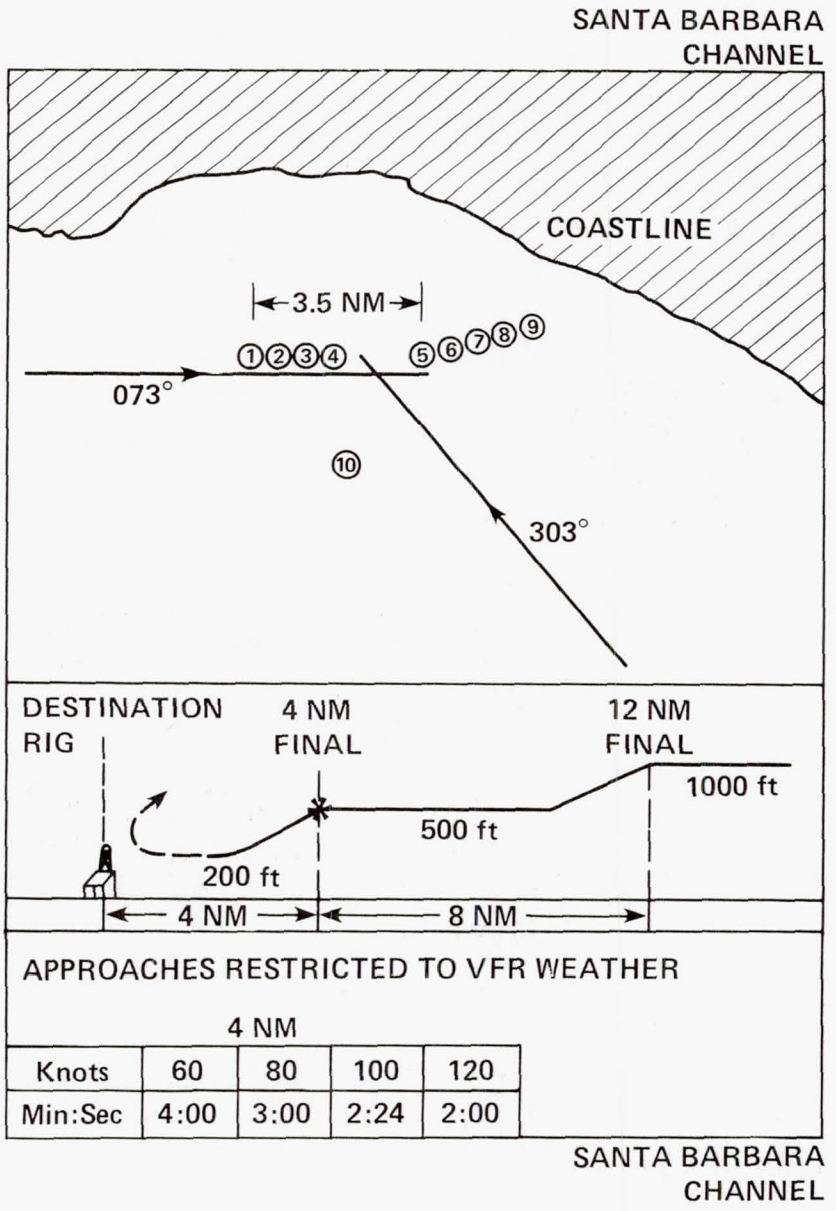

Figure 6. Location of oil rigs and flight approach profiles.

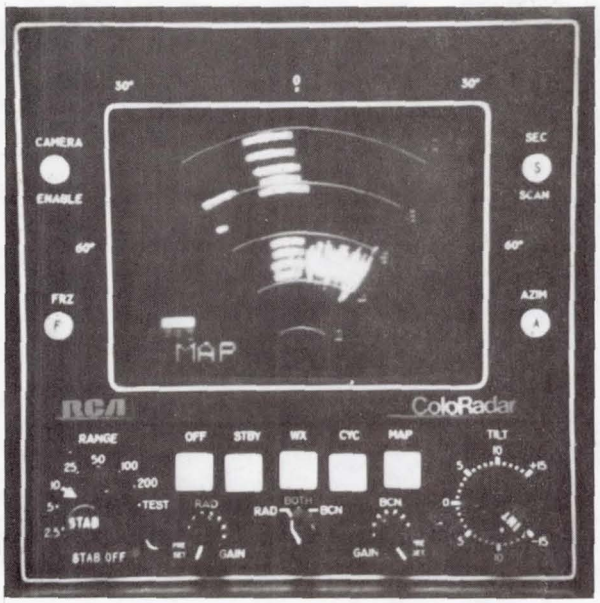

Simulated

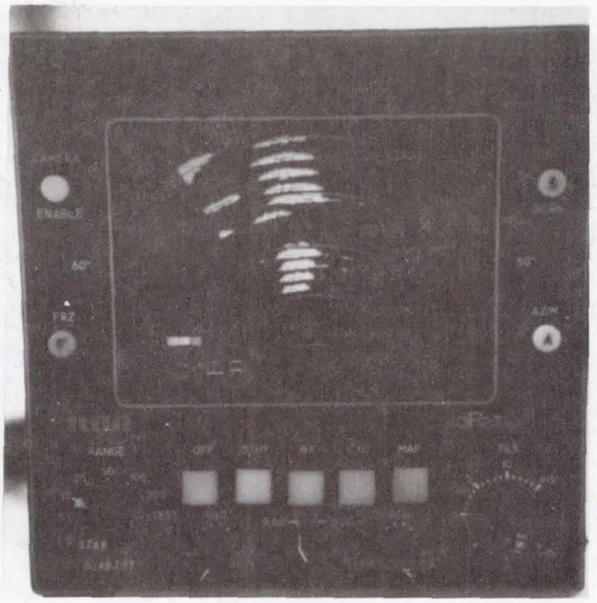

Actual

(a) MAP mode, 7.7 n. mi. west of rig 5, preset gain; altitude, 500 ft; heading, 076°; wind speed, 7 knots; wind direction, 180°; radar gain, 0; antenna tilt, 0.

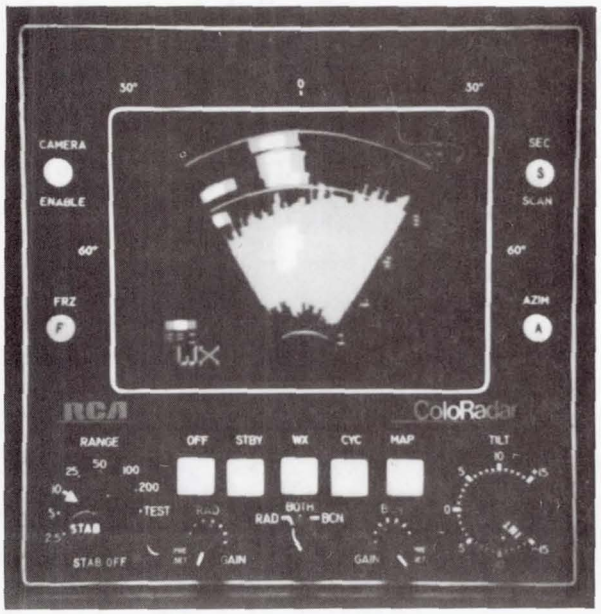

Simulated

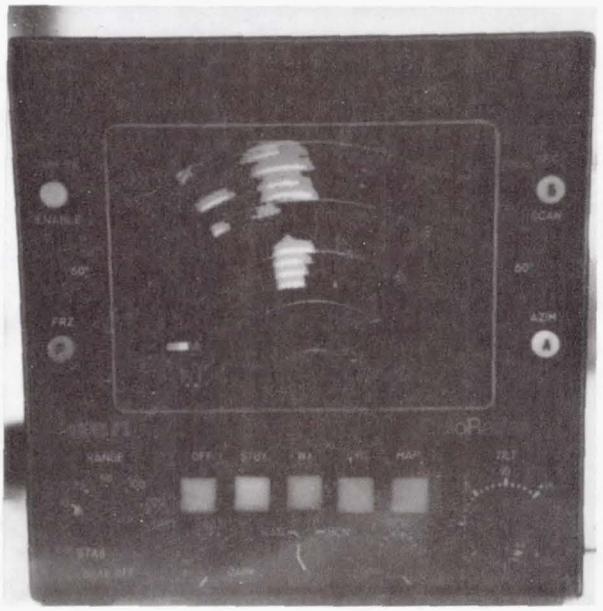

Actual

(b) WX mode, 8.2 n. mi. west of rig 5, preset gain; altitude, 500 ft; heading, 076°; wind speed, 7 knots; wind direction, 180°; radar gain, 0; antenna tilt, 0.

Figure 7.- Comparison of in-flight displays with simulated displays.

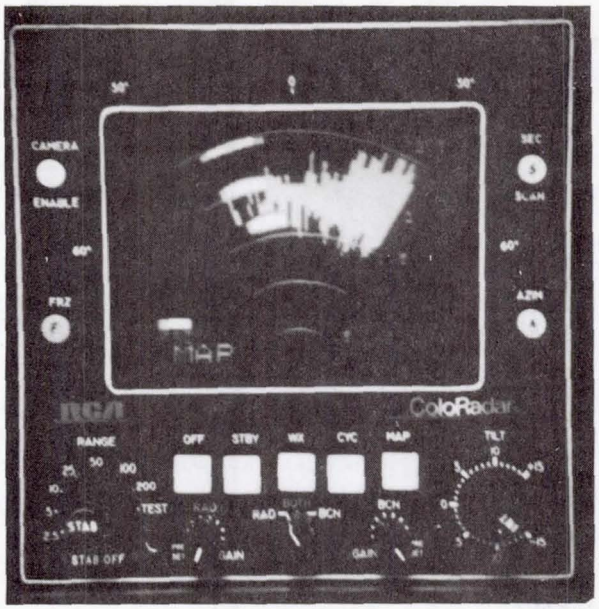

Simulated

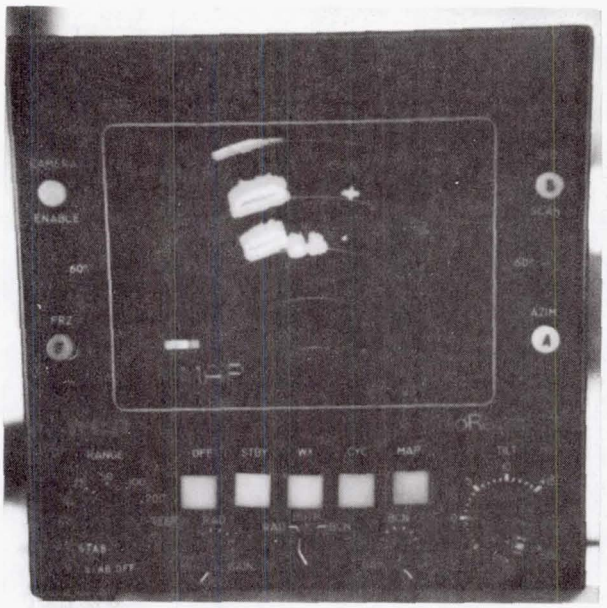

Actual

(c) MAP mode, 1.6 n. mi. west of rig 5, preset gain; altitude, 200 ft; heading, 083°; wind speed, 7 knots; wind direction, 180°; radar gain, 0; antenna tilt, 0.

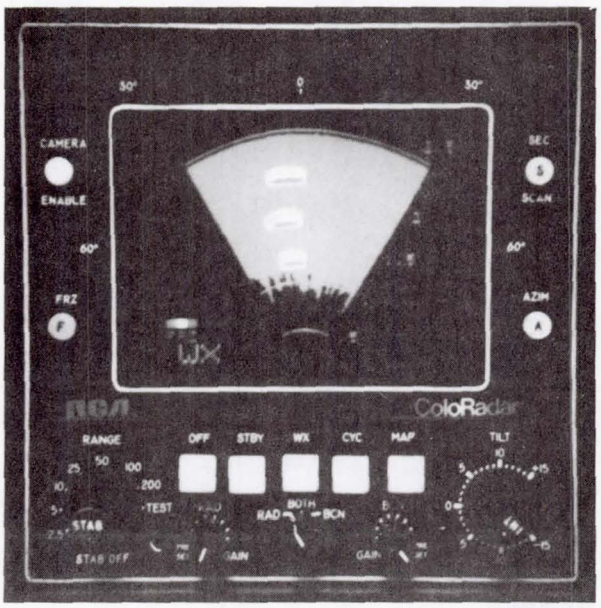

Simulated

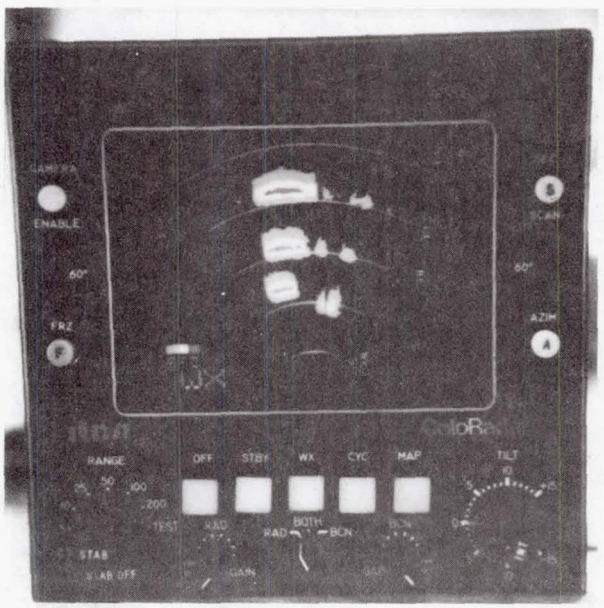

Actual

(d) WX mode, 1.2 n. mi. west of rig 5, preset gain; altitude, 200 ft; heading, 063°; wind speed, 7 knots; wind direction, 180°; radar gain, 0; antenna tilt, 0.

Figure 7.- Continued.

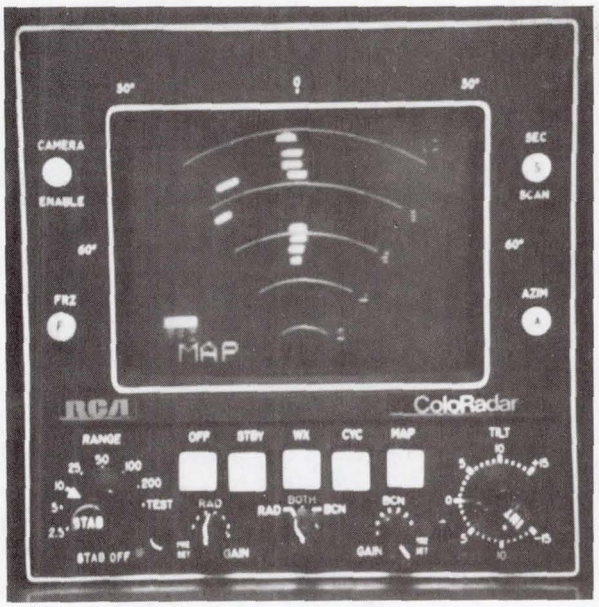

Simulated

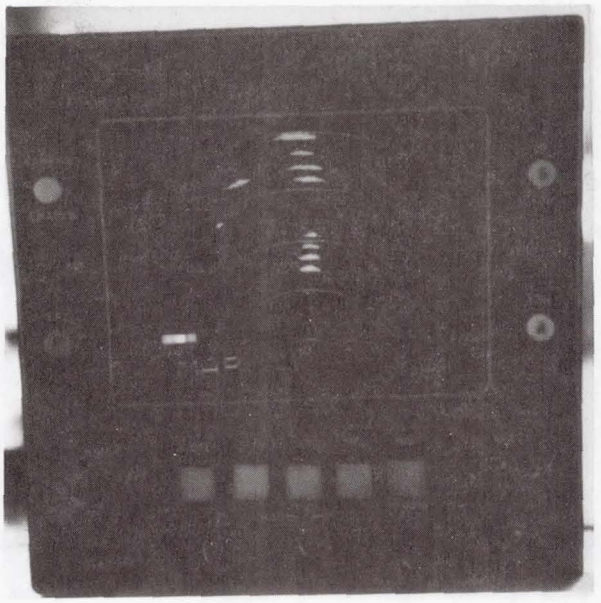

Actual

(e) MAP mode, 8.3 n. mi. west of rig 5, low gain; altitude, 1000 ft; heading, 073°; wind speed, 7 knots; wind direction, 180°; radar gain, -17 db; antenna tilt, 0.

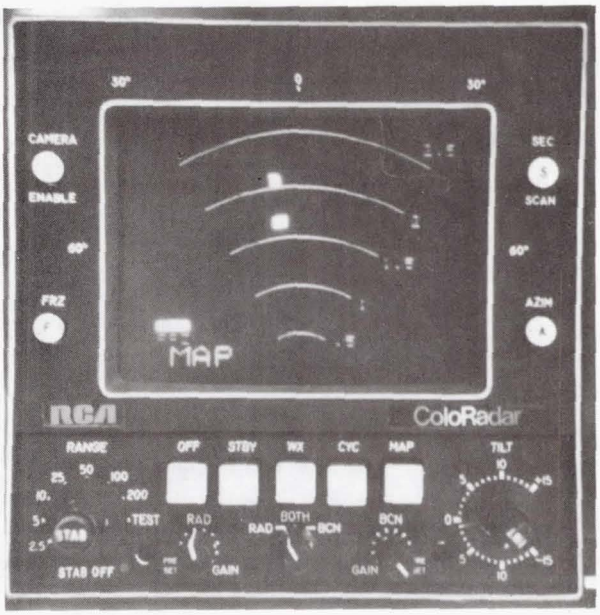

Simulated

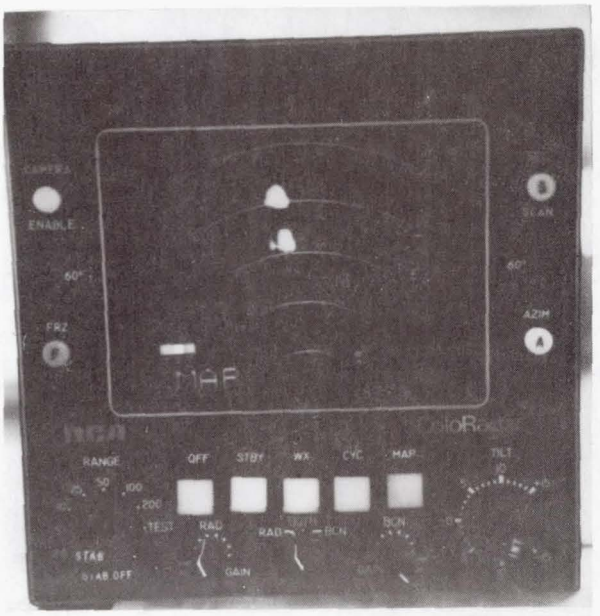

Actual

(f) MAP mode, 1.6 n. mi. west of rig 5, low gain; altitude, 200 ft; heading, 063°; wind speed, 7 knots; wind direction, 180°; radar gain, -22 dB; antenna tilt, -1°;

Figure 7.- Continued.

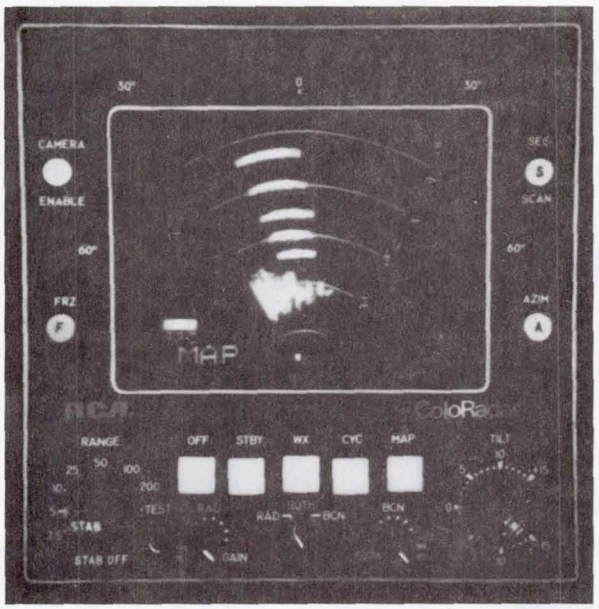

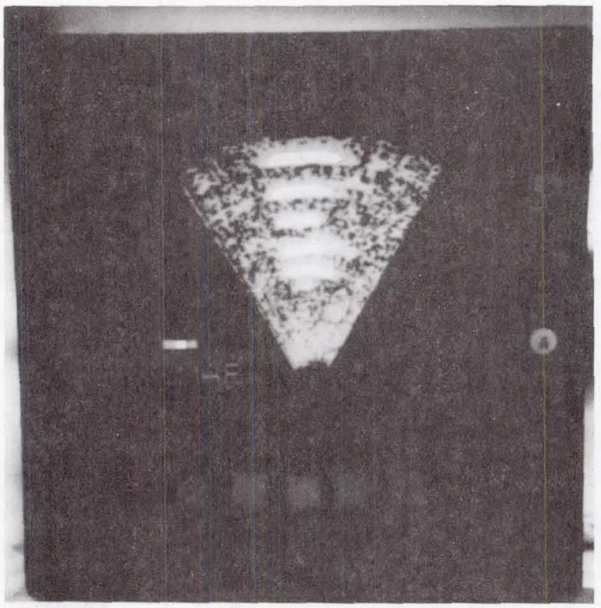

Simulated

Actual

(g) MAP mode, 2.5 n. mi. west of rig 5, maximum gain; altitude, 200 ft; heading, 068°; wind speed, 12 knots; wind direction, 240°; radar gain, 3 dB; antenna tilt, 0°.

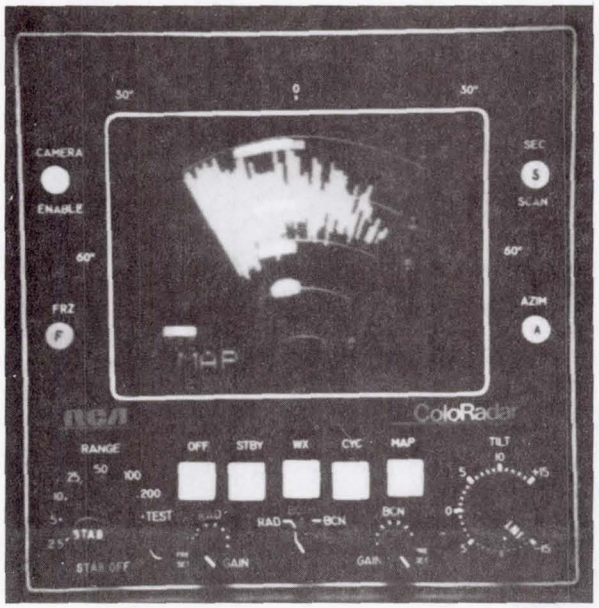

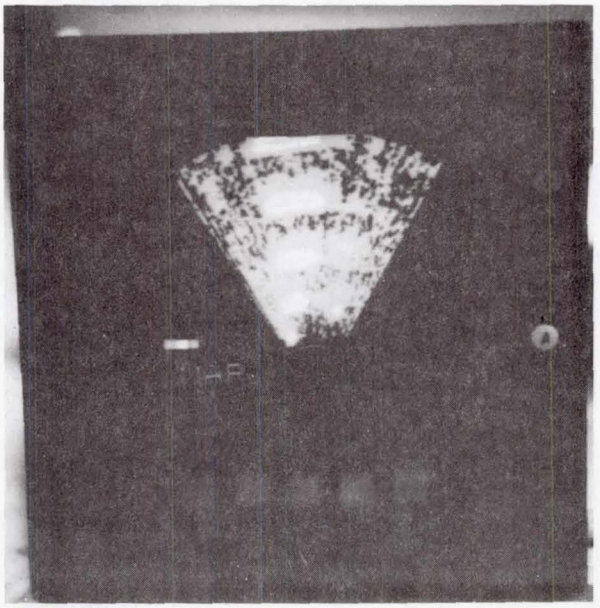

Simulated

Actual

(h) MAP mode, 0.9 n. mi. west of rig 5, maximum gain; altitude, 200 ft; heading, 0°; wind speed, 12 knots; wind direction, 240°; radar gain, 3 dB; antenna tilt, 0°.

Figure 7.- Continued.

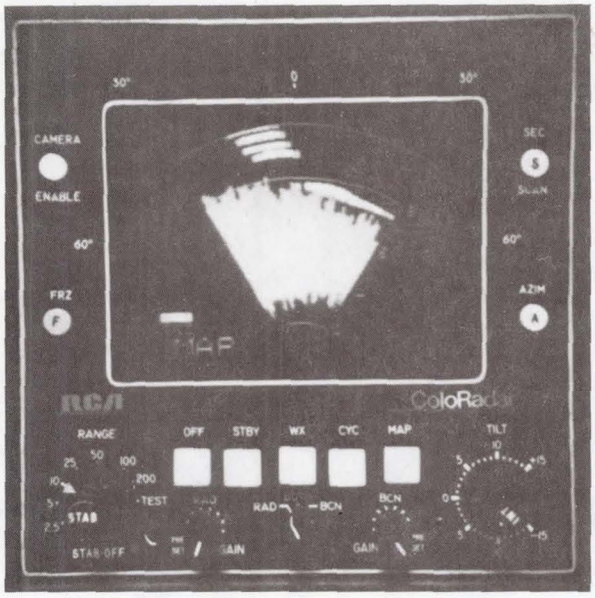

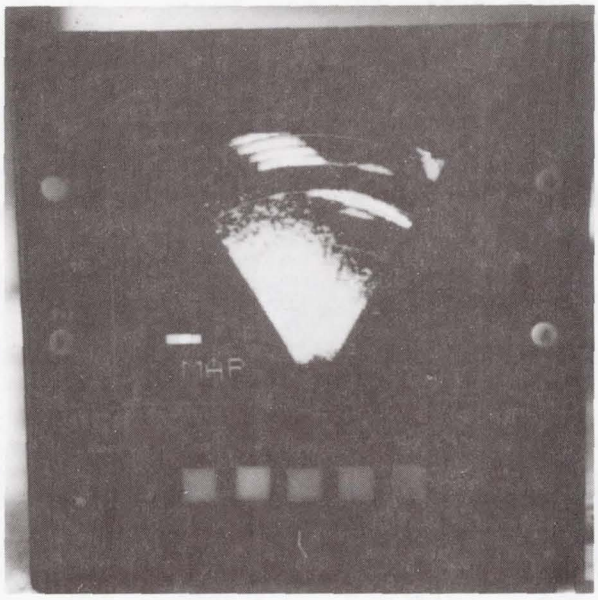

Simulated

Actual

(i) MAP mode, 9 n. mi. southeast of rig 4, preset gain; altitude, 500 ft; heading, 306°. wind speed, 12 knots; wind direction, 240°; radar gain, 0; antenna tilt, 0.

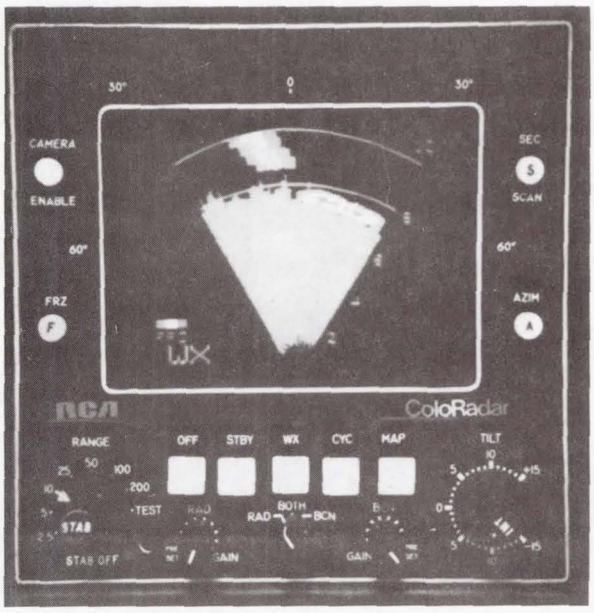

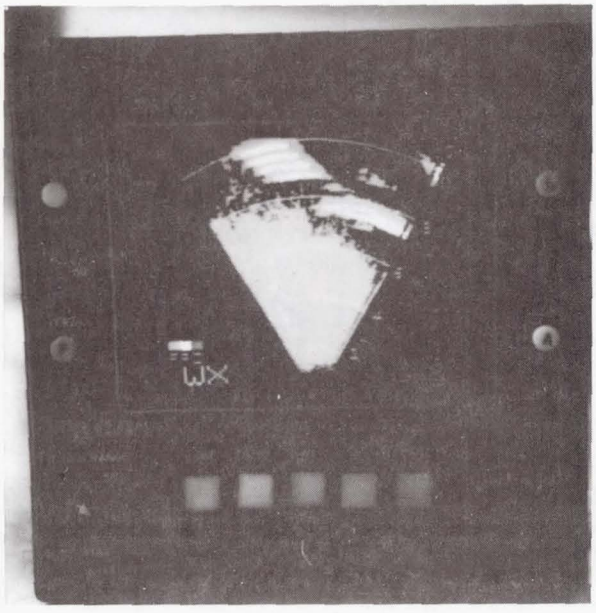

Simulated

Actual

(j) WX mode, 8.5 n. mi. southeast of rig 4, present gain; altitude, 500 ft; heading, 306°; wind speed, 12 knots; wind direction, 240°; radar gain, 0; antenna tilt, -1°.

Figure 7.- Continued.

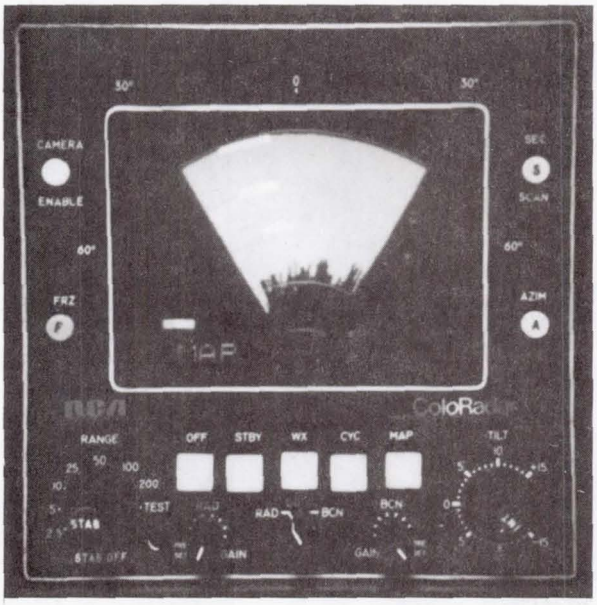

Simulated

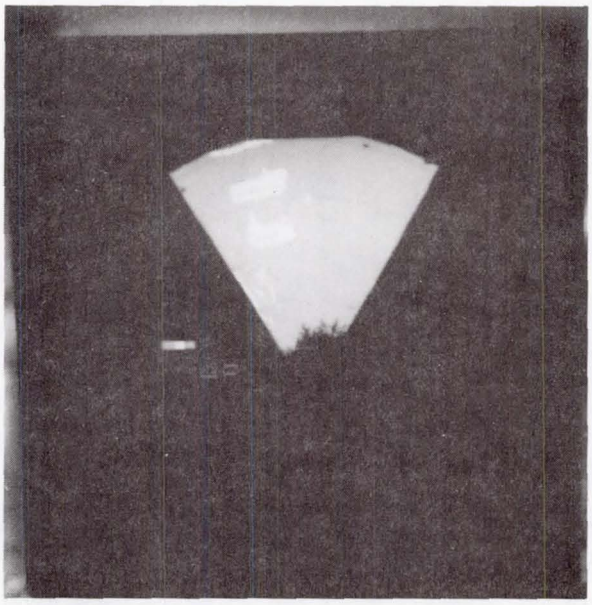

Actual

(k) MAP mode, 1.6 n. mi. southeast of rig 4, preset gain; altitude, 200 ft; heading, 283°; wind speed, 12 knots; wind direction, 240°; radar gain, 0; antenna tilt, 0.

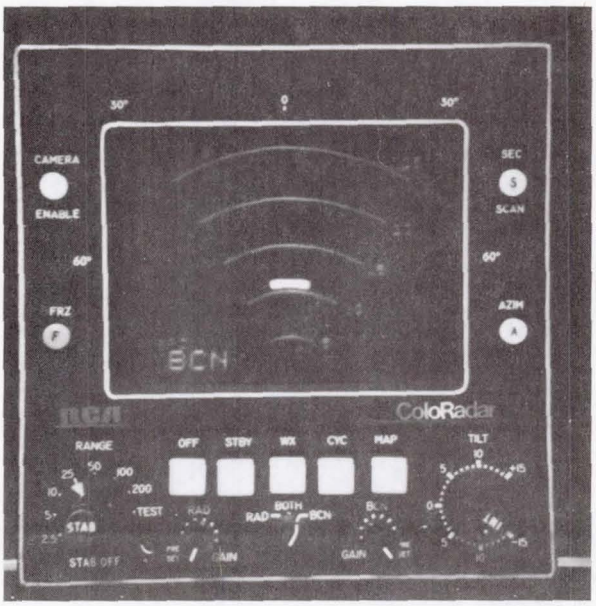

Simulated

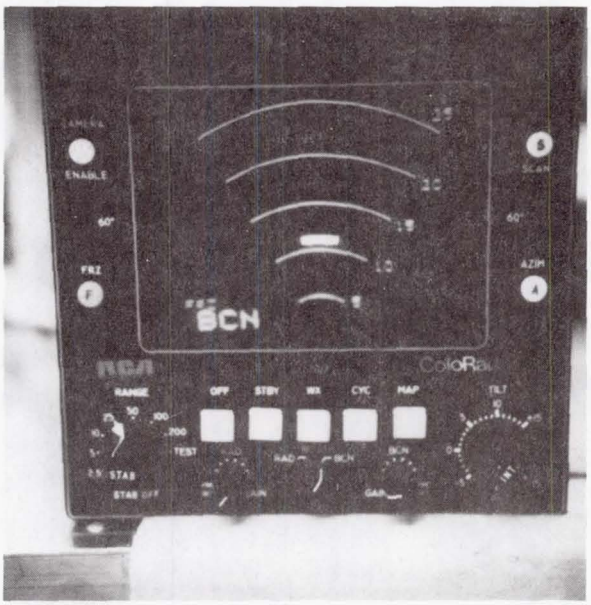

Actual

(l) Beacon mode, 10.5 n. mi. away from the beacon; altitude, 4500 ft; heading, 360°; beacon gain, 0; antenna tilt, -4°.

Figure 7.- Concluded.

1. Report No.	2. Government Accession No.	3. Recipient's Catalog No.
NASA TM-84315		

4. Title and Subtitle	5. Report Date
SIMULATION OF A WEATHER RADAR DISPLAY FOR OVER-WATER AIRBORNE RADAR APPROACHES	February 1983
	6. Performing Organization Code
7. Author(s)	8. Performing Organization Report No.
George R. Clary	A-9185
	10. Work Unit No.
9. Performing Organization Name and Address	T-3771
NASA Ames Research Center Moffett Field, Calif. 94035	11. Contract or Grant No.
	13. Type of Report and Period Covered
12. Sponsoring Agency Name and Address	Technical Memorandum
National Aeronautics and Space Administration Washington, D.C., 20546	14. Sponsoring Agency Code 532-01-11

15. Supplementary Notes

Point of Contact: George R. Clary, Ames Research Center, MS 210-9, Moffett Field, CA 94035, (415)965-5452 or FTS 448-5452

16. Abstract

Airborne radar approach (ARA) concepts are being investigated as a part of NASA's Rotorcraft All-Weather Operations Research Program on advanced guidance and navigation methods. This research is being conducted using both piloted simulations and flight test evaluations. For the piloted simulations, a mathematical model of the airborne radar has been developed for over-water ARAs to offshore platforms. This simulated flight scenario requires radar simulation of point targets, such as oil rigs and ships, distributed sea clutter, and transponder beacon replies. Radar theory, weather radar characteristics, and empirical data derived from in-flight radar photographs are combined to model a civil weather/mapping radar typical of those used in offshore rotorcraft operations. The resulting radar simulation is realistic and provides the needed simulation capability for ongoing ARA research.

17. Key Words (Suggested by Author(s))	18. Distribution Statement
Radar simulation Airborne radar approach Weather/mapping radar Piloted simulation	Unlimited Subject Category - 01

19. Security Classif. (of this report)	20. Security Classif. (of this page)	21. No. of Pages	22. Price*
Unclassified	Unclassified	27	A03

*For sale by the National Technical Information Service, Springfield, Virginia 22161